Available online at www.sciencedirect.com

ScienceDirect

Procedia CIRP 79 (2019) 101–106

www.elsevier.com/locate/procedia

12th CIRP Conference on Intelligent Computation in Manufacturing Engineering, 18-20 July 2018, Gulf of Naples, Italy

Machining induced residual stresses in AlSi10Mg component produced by Laser Powder Bed Fusion (L-PBF)

Gabriele Piscopo[a,]*, Eleonora Atzeni[a], Flaviana Calignano[a], Manuela Galati[a], Luca Iuliano[a], Paolo Minetola[a], Alessandro Salmi[a]

[a]*Politecnico di Torino, Department of Management and Production Engineering (DIGEP), C.so Duca degli Abruzzi, 24, 10129 Torino, Italy*

* Corresponding author. Tel.: +39-011-090-7280; fax: +39-011-090-7299. E-mail address: gabriele.piscopo@polito.it

Abstract

The adoption of metal powder-based laser process (L-PBF) for industrial applications continues to widen, due to an increasing knowledge on additive processes and the availability of new systems for industrial production. The use of L-PBF processes requires a deeper investigation and comparison on mechanical properties of conventional and additive parts. For instance, metal parts produced by L-PBF could require additional machining operations, which alter the stress state of additive components. In this work, the effect of machining operations on the residual stress state of an AlSi10Mg component produced by L-PBF is investigated by means of the semi destructive hole-drilling method.

Peer-review under responsibility of the scientific committee of the 12th CIRP Conference on Intelligent Computation in Manufacturing Engineering.

Keywords: Residual stresses; Laser Powder Bed Fusion; AlSi10Mg; Hole-drilling method; Machining.

1. Introduction

Additive Manufacturing (AM) is a manufacturing process that allows producing near net shaping parts with complex shapes without the use of expensive tools or equipment. The production of the parts occurs depositing the material layer by layer in contrast to the conventionally manufacturing processes, like milling and turning, in which the parts are produced by eliminating the materials by means of a cutting tool.

The AM technologies include several processes but for the industry field the Laser Powder Bed Fusion (L-PBF) also known as Selective Laser Melting (SLM) or Direct Metal Laser Sintering (DMLS) is the most used [1] and effective process to produce metal parts [2-4]. In the recent years the application of L-PBF in the industry grows rapidly [5,6] and the main application areas were the biomedical [7,8], the aerospace [9], the automotive [10] and the aeronautical ones [11]. Atzeni and Salmi [12] in 2012 demonstrated that the production using L-PBF is convenient for small and medium productivity. Although the numerous application of AM some issue as the limited materials available, the poor accuracy of the part and the presence of residual stresses has to be investigated [13]. L-PBF is an AM process in which a laser is used to melt a thin layer of the pre-placed bed of metal powder according with the CAD geometry of the part. Repeating the process is it possible to produce parts with complex geometries. Due to the nature of the energy source, during the process a large amount of residual stresses were generated [14]. Two different phenomena that generate residual stresses can be noticed. The first phenomenon is called Temperature Gradient Mechanism (TGM) and it was caused by the huge thermal gradient around the laser spot. It causes the expansion of the upper material due to the temperature rise, but this expansion is inhibited by the underlying material so a compressive strain is induced. The second phenomenon is the cool-down face of the molten top layer. In this case, when the molten material solidifies it tends to shrink, but this thermal contraction is prevented by the underlying layer, so a tensile stress is induced.

Residual stresses can cause distortion during the fabrication causing the failure of the process. Moreover, the deformations can occur when the component is complete and if the level of these deformations is higher than the design value they could

2212-8271
Peer-review under responsibility of the scientific committee of the 12th CIRP Conference on Intelligent Computation in Manufacturing Engineering.
10.1016/j.procir.2019.02.019

Nomenclature

F_t	tangential force components (N)
F_r	radial force components (N)
F_a	axial force components (N)
F_x	X force components (N)
F_y	Y force components (N)
F_z	Z force components (N)
h_0	undeformed chip thickness (mm)
d	depth of cut (mm)
w	width of cut (mm)
fz	feed per tooth (mm/tooth)
vc	cutting speed (m/min)
k_s	specific cutting pressure (MPa)
k_{s0}, z	constant and exponent of the specific cutting pressure
γ	rake angle (°)
γ_r	radial rake angle (°)
γ_a	axial rake angle (°)
χ	lead angle of the cutter (°)
φ	angular position of the cutter (°)

make the component unusable. Several studies were performed in order to understand and predict the residual stresses distribution in the produced component. Kruth and Mercelis [14] proposed a simple theoretical model to predict the residual stress distribution in a simple rectangular geometry. Shiomi et al. [15] performed an experimental investigation of residual stresses and showed that the heat treatment, the heating of the substrate and the re-scanning process reduced the residual stresses. Gusarov et al. [16] proposed a mathematical model for the prediction of residual stresses and showed that the residual stresses in the scanning direction are approximatively half of the residual stresses measured in the transversal direction. Liu et al. [17] studied the effect of energy input and scanning track length on residual stress distribution and showed that lower energy input and small track length reduce residual stresses. Mugwagwa et al. [18] studied the effect of laser power, scanning speed and layer thickness on the residual stresses. In 2017, Salmi et al. [19] performed and experimental analysis on residual stresses in different phases of the production process and the effect of support structures, thermal treatment and shot-peening process were investigated. In 22018 the same authors [20] performed an experimental analysis in which the effect of part orientation on residual stress distribution was examined.

The surface roughness (R_a) surfaces of the components produced by L-PBF varies between 8 µm and 30 µm [21-23] and this value depends on several factors like material, process parameters and part orientation. The commonly industrial application requires a surface quality of 0.8 µm in order to avoid premature failure of the parts due to initiating of cracks [24]. Hence, final machining operations were required in order to obtain the desired quality. It is well known that cutting processes as turning and milling induce residual stresses on the machined surface [25-27]. El-Khabeery and Fattouh [28] studied the effect of cutting speed, feed rate and depth of cut on the residual stress distribution during the milling operation. Denkena and De Leon [29] investigated the effect of machining parameters, cooling strategy and the cutting tool geometry on the induced residual stresses in aluminium component.

In this work the residual stress distribution on AlSi10Mg component produced by L-PBF and subsequently subjected to milling operation was examined. The residual stresses were evaluated using the hole drilling strain gauge method.

2. Materials and method

AlSi10Mg alloy has been selected for this study. Residual stresses after machining operations on AM components are evaluated and compared with conventional cast parts of same material subjected to analogous operations. A shoulder face milling operation is adopted in the tests. The machining operations and cutting force evaluation are explained in detail in the following sections. The methodology adopted to measure and evaluate the residual stresses is also illustrated briefly.

2.1. Test specimens

Two aluminum alloy specimens were produced in a single job using an EOSINT M 270 Dual Mode machine. This machine uses a 200 W fiber laser, with a wavelength of 1060-1100 nm, focused on a 0.1 mm diameter to melt the metallic powder. The layer was 30 µm thick and the building platform was kept at 100 °C. The dimensions of the samples were 30 × 20 × 15 mm³. The components were constructed while blowing Argon into the work chamber in order to avoid oxidation of the material. A standard scanning strategy, which foresees different exposition parameters for the core, the skin, and the contour, was adopted. The samples were subjected to a stress relieving thermal treatment at 300°C for 3 h and then removed from the platform. After the post-processing operation, a sample was measured in order to evaluate the final residual stress state. The second specimen was used to test the effect of milling operation on the residual stresses. An additional aluminum alloy specimen (80 × 80 × 15 mm³) produced by conventional sand casting and shot-peened was tested for comparison. This specimen is referred as *reference*.

2.2. Face milling and analytical prediction of cutting forces

In face milling the resultant cutting force can be resolved into the tangential, axial and radial directions of the cutter. The three components are expressed in general form as:

$$F_t = k_s \cdot h_0 \cdot d \tag{1}$$

where k_s is the specific cutting pressure, h_0 is the chip thickness and d is the depth of cut. The force coefficient is dependent on cutting condition and work material and can be expressed as:

$$K_s = k_{s0} \cdot {h_0}^{-z} \cdot (1 - 0.01 \cdot \gamma) \tag{2}$$

where γ is the rake angle.
The chip thickness h_0 in face milling operation can be approximated as:

$$h_0 = f_z \cdot \sin\chi \cdot \sin\varphi \tag{3}$$

where χ is the lead angle of the cutter, and φ is the angular position of the cutter.

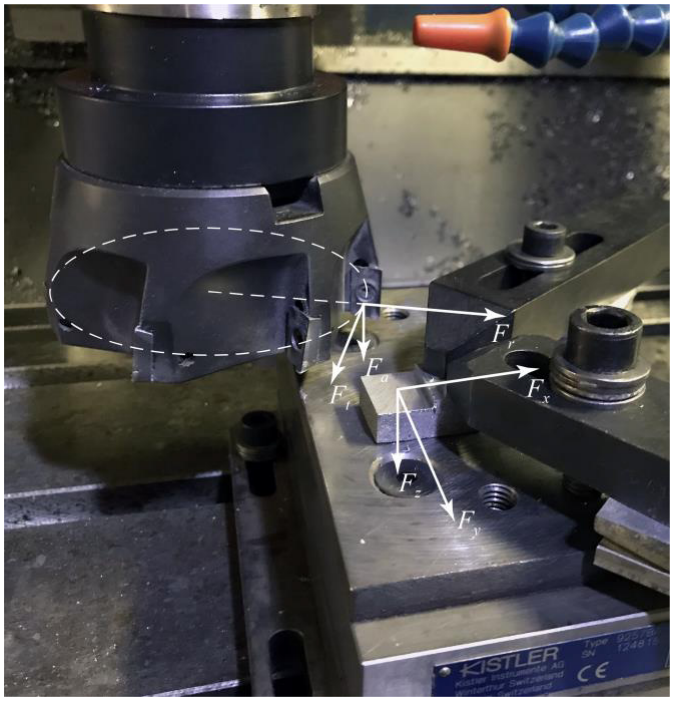

Fig. 1. Force acquisition system in face milling operation.

The radial force can be expressed by the experimental equation:

$$F_r = F_t \cdot (0.44 - 0.013\gamma_r) \quad (4)$$

where γ_r is the radial rake angle of the cutting edge.
The axial force can be expressed by the experimental equation [30]:

$$F_a = F_t \cdot \frac{f_z + d \cdot \cot\chi}{d} (0.88 - 0.013\gamma_a) \quad (5)$$

where γ_a is the axial rake angle.
The force components in the directions of the machine tool axes are calculated by applying the transformations:

$$\begin{bmatrix} F_x \\ F_y \\ F_z \end{bmatrix} = \begin{bmatrix} \cos\varphi & -\sin\varphi & 0 \\ \sin\varphi & \cos\varphi & 0 \\ 0 & 0 & 1 \end{bmatrix} \begin{bmatrix} F_t \\ F_r \\ F_a \end{bmatrix} \quad (6)$$

2.3. Machining tests

A 90° shoulder face milling cutter with a diameter of 100 mm and seven (APKT160408A-2C) rectangular inserts were used in milling the aluminum alloy specimens. The rake angle is 24° and the axial (inclination) angle is 5°. A quartz 3-component Kistler Type 9257BA dynamometer was fixed on the table of the three-axis machine tool and each specimen was fastened on it to measure reaction forces during machining. The force data were collected by means of a sampling device installed on a PC. A National Instruments acquisition board with a 16-Bit resolution, 1 MS/s multichannel, and 16 analogic inputs was used. The signals were sampled at the frequency of 5,000 Hz. The data were acquired and elaborated using program developed in LabVIEW 2017.

The acquired data were analyzed, and the frequency response was observed to determine the resonance peaks. The frequency signals corresponding to the rotation frequency of the milling cutter and to its multiples were filtered using a band-stop filter. Moreover, a smoothing was applied, and the moving average was set equal to 20. The thus obtained signal describes the trend of the force components during the test. The experimental set-up is shown in Fig. 1. Cutting conditions are shown in Table 1.

Table 1. Cutting conditions for milling tests

	depth of cut d *(mm)*	width of cut w *(mm)*	cutting speed v_c *(m/min)*	feed per tooth f_z *(mm/tooth)*	mode of milling
2 passes	1	15	380	0.2	down

2.4. Residual stresses measurements

The MTS3000 RESTAN (Fig. 2) system by SINT Technology, which is based on the hole-drilling strain gauge method, was used to measure the residual stresses, according to the ASTM E837-13a standard [31]. A 2 mm diameter drill bit was used to produce a 1.2 mm deep flat-bottom hole, with a sequence of 24 drilling steps of 50 µm. A K-RY61-1.5/120R rosette strain gauge made by HBM was used during the experimental campaign. The surface of each specimen was prepared for the application of the rosette strain gauge through sanding with a 200 grain abrasive paper and then with a 400

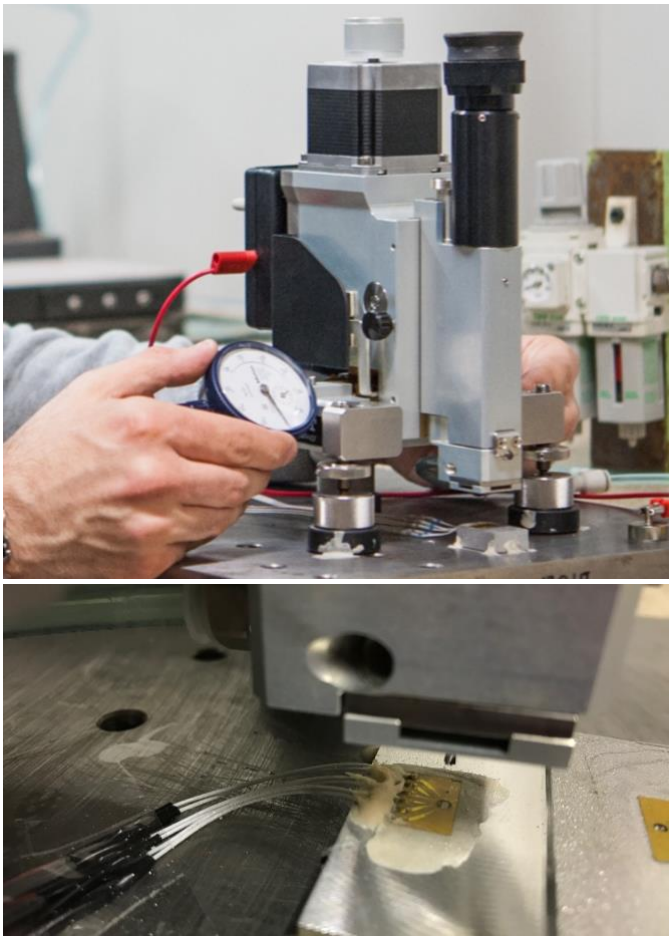

Fig. 2. MTS3000 RESTAN (REsidual STress ANalyzer) system by SINT Technology during a measurement phase.

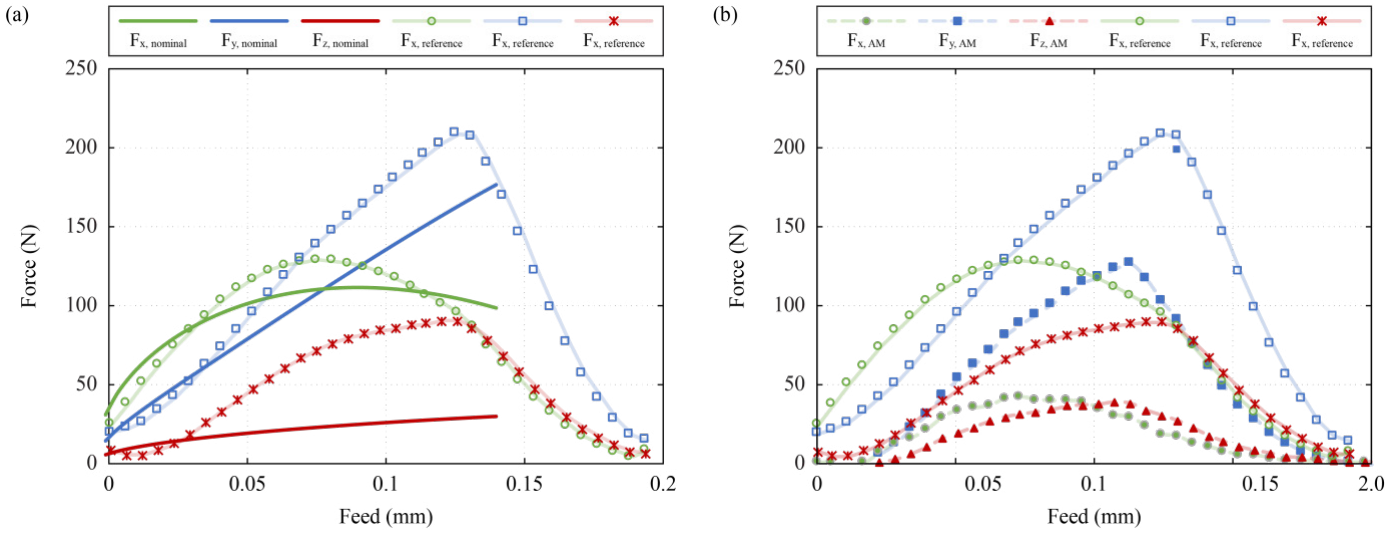

Fig. 3. Cutting forces trends predicted and measured on the (a) reference specimen and on the (b) AM specimen.

grain abrasive paper. Finally, it was cleaned with an RMS1 Spray solvent. LabVIEW 2017 was used to develop an acquisition program to automate the data acquisition and to compute residual stresses according to ASTM E837-13a [32].

3. Results and discussion

The results of the experimental tests and numerical elaborations are presented hereafter.

3.1. Cutting forces

The directions X, Y and Z force components measured on the reference specimen are shown in Fig. 3(a). The approximate trends of measured and predicted cutting forces are in reasonable agreement. The axial component F_z resulted higher than the predicted one, probably due to the effect of the nose radius of the insert. A compressive load of around 90 N is exerted on the surface of the part. The force components measured on the AM specimen during milling operation, illustrated in Fig. 3(b), exhibit the same trend of the reference specimen, even if their values are lower. Especially, the axial component of the force is about 40 N.

3.2. Residual stresses

Residual stresses were measured before machining tests on both the reference and the AM specimen. In the reference specimen a 0.5 mm deep compressive profile is observed, Fig. 4(a) Below the compressive layer, the tensile state tends to zero. Fig. 4b shows residual stresses of the AM specimen; a low superficial tensile state, for a depth of about 1 mm, is still present after the heat treatment. The maximum value of the stress is 100 MPa.

The residual stress profiles after machining are shown in Fig. 5(a) and Fig. 5(b) for the reference and the AM specimen respectively. The machining operation, by cutting 2 mm of material, removed the subsurface layer subjected to compressive or tensile stress. Consequently, the residual stresses after machining tests should be mainly due to the machining loads. From Fig. 4 and Fig. 5, it is possible to observe that the stress profiles on the two specimens have a similar trend. A surface tensile stress and a subsurface compressive state is induced by the milling operation. Higher compressive stress is induced in the reference specimen. In this specimen, the stress drops rapidly from a tensile stress of 60 MPa to a compressive stress of 50 MPa within the first

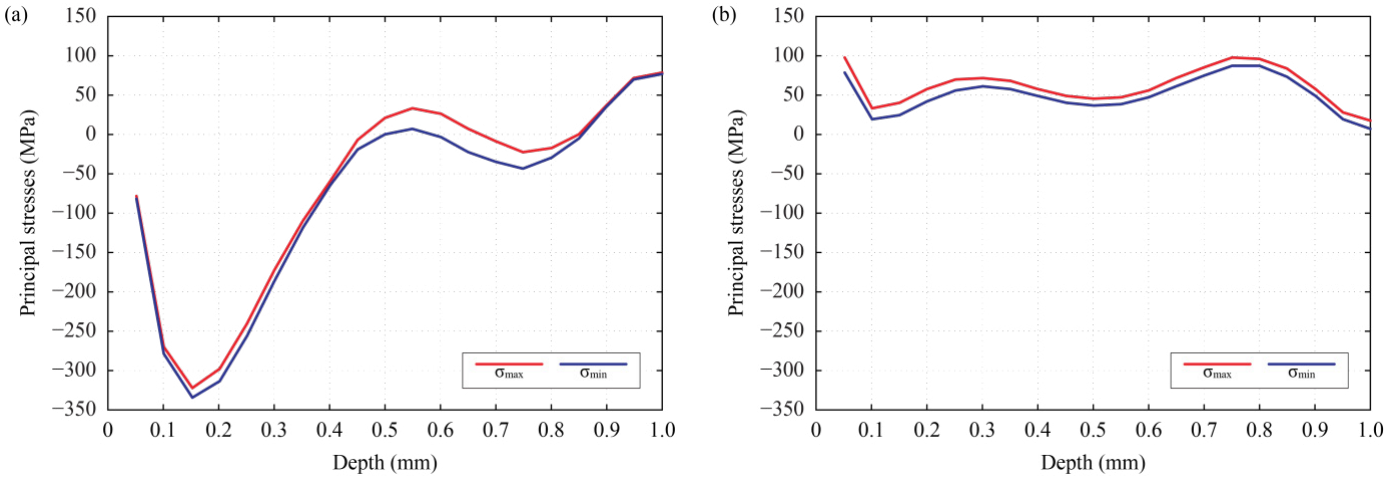

Fig. 4. Residual stress distribution before machining in the (a) reference specimen and in the (b) AM specimen.

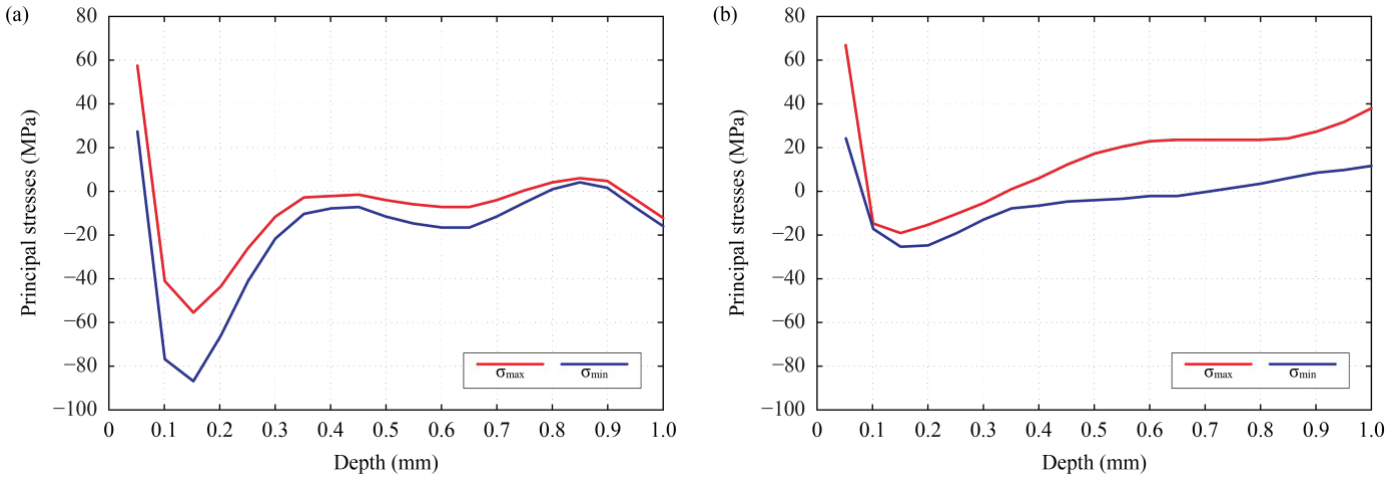

Fig. 5. Residual stress distribution after machining in the (a) reference specimen and in the (b) AM specimen.

150 µm, and then it approaches zero at about 300 µm below the machined surface. Considering the AM specimen, analogously to the reference case, a rapid drop of the stress is observed from a tensile value of 60 MPa to a compressive peak of 20 MPa at 150 µm. At larger depths, the compressive residual stress decreases, and beyond 300 µm a low tensile stress is observed, probably remained after the thermal relieving treatment of the specimen.

4. Conclusions

The surface residual stresses and subsurface residual stress distributions induced by face milling on an AlSi10Mg sample manufactured by laser powder bed fusion were investigated by hole-drilling method. The main observations are summarized below:

- the oblique cutting process and the geometry of the insert cause an axial compressive force on the surface of the specimen;
- a surface tensile stress and a subsurface compressive state is induced by the milling operation;
- the compressive stress on the AM part is lower than that induced on a conventional part of same material;
- higher force increases the subsurface compressive state and penetration depth.

Acknowledgements

The authors would like to thank Mr. Giovanni Marchiandi for his assistance during the measurement phase and data elaboration.

References

[1] Wohlers TT, Associates W. Wohlers Report 2015: Additive Manufacturing and 3D Printing State of the Industry : Annual Worldwide Progress Report: Wohlers Associates; 2015.
[2] Seabra M, Azevedo J, Araújo A, Reis L, Pinto E, Alves N, Santos R, Mortágua JP. Selective laser melting (SLM) and topology optimization for lighter aerospace componentes. Procedia Structural Integrity. 2016;1:289-96.
[3] Wang M, Wu Y, Lu S, Chen T, Zhao Y, Chen H, Tang Z. Fabrication and characterization of selective laser melting printed Ti–6Al–4V alloys subjected to heat treatment for customized implants design. Progress in Natural Science: Materials International. 2016;26:671-7.
[4] Li Z, Zhang DZ, Dong P, Kucukkoc I. A lightweight and support-free design method for selective laser melting. The International Journal of Advanced Manufacturing Technology. 2017;90:2943-53.
[5] Petrovic V, Vicente Haro Gonzalez J, Jordá Ferrando O, Delgado Gordillo J, Ramón Blasco Puchades J, Portolés Griñan L. Additive layered manufacturing: sectors of industrial application shown through case studies. International Journal of Production Research. 2011;49:1061-79.
[6] Gibson I. The changing face of additive manufacturing. Journal of Manufacturing Technology Management. 2017;28:10-7.
[7] Zhang LC, Klemm D, Eckert J, Hao YL, Sercombe TB. Manufacture by selective laser melting and mechanical behavior of a biomedical Ti–24Nb–4Zr–8Sn alloy. Scripta Materialia. 2011;65:21-4.
[8] Mullen L, Stamp RC, Brooks WK, Jones E, Sutcliffe CJ. Selective Laser Melting: A regular unit cell approach for the manufacture of porous, titanium, bone in - growth constructs, suitable for orthopedic applications. Journal of Biomedical Materials Research Part B: Applied Biomaterials. 2009;89:325-34.
[9] Liu R, Wang Z, Sparks T, Liou F, Newkirk J. 13 - Aerospace applications of laser additive manufacturing A2 - Brandt, Milan. Laser Additive Manufacturing: Woodhead Publishing; 2017. p. 351-71.
[10] Song Y, Yan Y, Zhang R, Xu D, Wang F. Manufacture of the die of an automobile deck part based on rapid prototyping and rapid tooling technology. Journal of Materials Processing Technology. 2002;120:237-42.
[11] Chantarapanich N, Laohaprapanon A, Wisutmethangoon S, Jiamwatthanachai P, Chalermkarnnon P, Sucharitpwatskul S, Puttawibul P, Sitthiseripratip K. Fabrication of three-dimensional honeycomb structure for aeronautical applications using selective laser melting: A preliminary investigation. Rapid Prototyping Journal. 2014;20:551-8.
[12] Atzeni E, Salmi A. Economics of additive manufacturing for end-usable metal parts. The International Journal of Advanced Manufacturing Technology. 2012;62:1147-55.
[13] Huang Y, Leu MC, Mazumder J, Donmez A. Additive manufacturing: current state, future potential, gaps and needs, and recommendations. Journal of Manufacturing Science and Engineering. 2015;137:014001.
[14] Mercelis P, Kruth J-P. Residual stresses in selective laser sintering and selective laser melting. Rapid prototyping journal. 2006;12:254-65.
[15] Shiomi M, Osakada K, Nakamura K, Yamashita T, Abe F. Residual stress within metallic model made by selective laser melting process. CIRP Annals-Manufacturing Technology. 2004;53:195-8.
[16] Gusarov AV, Pavlov M, Smurov I. Residual Stresses at Laser Surface Remelting and Additive Manufacturing. Physics Procedia. 2011;12:248-54.
[17] Liu Y, Yang Y, Wang D. A study on the residual stress during selective laser melting (SLM) of metallic powder. The International Journal of Advanced Manufacturing Technology. 2016;87:647-56.
[18] Mugwagwa L, Dimitrov D, Matope S, Yadroitsev I. Influence of process

parameters on residual stress related distortions in selective laser melting. Procedia Manufacturing. 2018;21:92-9.
[19] Salmi A, Atzeni E, Iuliano L, Galati M. Experimental analysis of residual stresses on AlSi10Mg parts produced by means of Selective Laser Melting (SLM). Procedia CIRP. 2017;62:458-63.
[20] Salmi A, Piscopo G, Atzeni E, Minetola P, Iuliano L. On the Effect of Part Orientation on Stress Distribution in AlSi10Mg Specimens Fabricated by Laser Powder Bed Fusion (L-PBF). Procedia CIRP. 2018;67:191-6.
[21] Strano G, Hao L, Everson RM, Evans KE. Surface roughness analysis, modelling and prediction in selective laser melting. Journal of Materials Processing Technology. 2013;213:589-97.
[22] Kruth JP, Froyen L, Van Vaerenbergh J, Mercelis P, Rombouts M, Lauwers B. Selective laser melting of iron-based powder. Journal of Materials Processing Technology. 2004;149:616-22.
[23] Delgado J, Ciurana J, Rodríguez CA. Influence of process parameters on part quality and mechanical properties for DMLS and SLM with iron-based materials. The International Journal of Advanced Manufacturing Technology. 2012;60:601-10.
[24] Dalgarno K. "Materials research to support high performance RM parts", Rapid Manufacturing 2nd International Conference, Loughborough University. 2007:147-56.
[25] Brinksmeier E, Cammett J, König W, Leskovar P, Peters J, Tönshoff H. Residual stresses—measurement and causes in machining processes. CIRP Annals-Manufacturing Technology. 1982;31:491-510.
[26] Jacobus K, DeVor RE, Kapoor SG. Machining-Induced Residual Stress: Experimentation and Modeling. Journal of Manufacturing Science and Engineering. 1999;122:20-31.
[27] Ee KC, Dillon OW, Jawahir IS. Finite element modeling of residual stresses in machining induced by cutting using a tool with finite edge radius. International Journal of Mechanical Sciences. 2005;47:1611-28.
[28] El-Khabeery MM, Fattouh M. Residual stress distribution caused by milling. International Journal of Machine Tools and Manufacture. 1989;29:391-401.
[29] Denkena B, De Leon L. Milling induced residual stresses in structural parts out of forged aluminium alloys. International Journal of Machining and Machinability of Materials. 2008;4:335-44.
[30] Pylkkinen J. Cuttin Forces in Face Millinq, University of Oulu, Department of Mechanical Engineering, 1984, p. 11.
[31] Vrancken B, Cain V, Knutsen R, Van Humbeeck J. Residual stress via the contour method in compact tension specimens produced via selective laser melting. Scripta Materialia. 2014;87:29-32.
[32] E837-13a A. Standard Test Method for Determining Residual Stresses by the Hole-Drilling Strain-Gage Method, ASTM International, West Conshohocken, PA, 2013, http://www.astm.org/.